Chemical Engineering Journal 512 (2025) 162419

Contents lists available at ScienceDirect

Chemical Engineering Journal

journal homepage: www.elsevier.com/locate/cej

In-situ electro-polymerization of aromatic diimide bridged N-phenylcarbazole as high-voltage cathode materials for long-lasting cationic and anionic co-storage batteries

Xinmei Song [a,1], Qianchuan Yu [a,1], Junjie Li [a], Zuoao Wu [a], Yizhi Xing [a], Yaoda Wang [a], Lina Qin [a], Huapeng Sun [b], Zuoxiu Tie [a,c,d,*], Jing Ma [a,*], Zhong Jin [a,c,d,e,*]

[a] State Key Laboratory of Coordination Chemistry, MOE Key Laboratory of Mesoscopic Chemistry, MOE Key Laboratory of High Performance Polymer Materials and Technology, Jiangsu Key Laboratory of Advanced Organic Materials, Suzhou Key Laboratory of Green Intelligent Manufacturing of New Energy Materials and Devices, Tianchang New Materials and Energy Technology Research Center, Institute of Green Chemistry and Engineering, School of Chemistry and Chemical Engineering, Nanjing University, Nanjing, Jiangsu 210023, PR China

[b] School of New Energy, Chenjiang Laboratory, Chenzhou Vocational Technical College, Chenzhou, Hunan 423000, PR China

[c] Nanjing Tieming Energy Technology Co. Ltd., Nanjing, Jiangsu 210093, PR China

[d] Suzhou Tierui New Energy Technology Co. Ltd., Suzhou, Jiangsu 215228, PR China

[e] Yoffe Products (Tianchang) Co., Ltd., Tiangchang, Anhui 239300, PR China

ARTICLE INFO

Keywords:
Rechargeable lithium batteries
Organic materials
π-Conjugated polymers
In situ electro-polymerization
Ultralong cycling life

ABSTRACT

Organic electrode materials with large π electron-deficient backbones and inherently electroactive functional groups hold great promise for serving as advanced cathode materials in secondary batteries. However, conventional organic cathodes were usually plagued by low specific capacity, poor electronic/ionic conductivity, and high solubility in electrolytes. In this study, we report an efficient molecule engineering strategy to incorporate N-phenylcarbazole (NPC) groups as N-substituents on both sides of aromatic diimides to obtain di(N-phenylcarbazole) naphthalene/benzene diimides (namely DNPC-XDI, where X = N, B). The introduced electron-deficient NPC groups could induce the in-situ electro-polymerization of DNPC-XDI under applied field conditions, and also function as p-type anion-storage sites to achieve exceptional cationic and anionic co-storage with significantly enhanced operation voltage, specific capacity and rate capability. Comprehensive characterizations unveiled that the Poly(DNPC-XDI) cathodes operate through a hybrid cation–anion co-redox mechanism, involving the loading/detaching of Li^+ cations on C=O functional groups and the concurrent doping/de-doping behavior of PF_6^- anions on Poly-carbazole backbones. The resultant Poly(DNPC-XDI) (X = N, B) displayed remarkable electrochemical performances, including a high cut-off voltage of 4.3 V and reversible specific capacities of 359.2 and 237.5 mAh g^{-1} at a current density of 100 mA g^{-1}. Impressively, even at a significantly higher current density of 10 A g^{-1}, the Poly(DNPC-XDI) (X = N, B) still maintained reversible specific capacities of 100.5 and 75.0 mAh g^{-1} after 10,000 cycles, confirming their outstanding rate performance and cycling stability. Theoretical calculations revealed that the lithiation process was energetically favourable and without the formation of π-π stacking structures. This study offers valuable insights into the rational design of molecular structures and efficient in-situ electrochemical polymerization methods for optimizing organic cathode materials to achieve high-performance cationic-anionic synergistic secondary batteries.

* Corresponding authors at: State Key Laboratory of Coordination Chemistry, MOE Key Laboratory of Mesoscopic Chemistry, MOE Key Laboratory of High Performance Polymer Materials and Technology, Jiangsu Key Laboratory of Advanced Organic Materials, Tianchang New Materials and Energy Technology Research Center, Research Institute of Green Chemistry and Engineering, School of Chemistry and Chemical Engineering, Nanjing University, Nanjing, Jiangsu 210023, PR China.

E-mail addresses: zxtie@nju.edu.cn (Z. Tie), majing@nju.edu.cn (J. Ma), zhongjin@nju.edu.cn (Z. Jin).

[1] These authors contributed equally to this work.

https://doi.org/10.1016/j.cej.2025.162419
Received 5 October 2024; Received in revised form 1 April 2025; Accepted 7 April 2025
Available online 10 April 2025

1. Introduction

Lithium-ion batteries (LIBs) have emerged as the predominant energy sources for portable devices and electric vehicles [1–4]. Currently, cathodes in commercially available LIBs are predominantly composed of inorganic materials that are not source-abundant or easy-to-process [5–7]. Alternatively, organic materials are being increasingly explored as active components in rechargeable batteries due to their lightweight nature, facile processability, and unlimited resource availability [8–11]. Especially, carbonyl compounds have garnered attention as potentially advantageous cathode materials. Aromatic imide compounds featuring multiple carbonyl groups have drawn significant interest due to their extensive π-conjugated framework and inherent redox-active properties. However, aromatic imides often face analogous challenges such as inherent electrical insulation high solubility in organic electrolytes [12–14], and low capacity [15]. Several methods have been devised to regulate the molecular frameworks of aromatic imides, encompassing polymerization processes that link monomers into polymeric chains [16–19], the introduction of substituents to modify electronic properties [20–24], the extension of the aromatic conjugation network for enhanced delocalization [25–27], and the creation of non-topographic structural arrangements [28–32]. Despite considerable research aimed at boosting the performance of batteries utilizing aromatic imides, there remains a significant gap in the development of straightforward synthetic methodologies that simultaneously deliver outstanding specific capacity, rate capability, and electrochemical stability.

Cationic and anionic co-storage strategy, which involves the co-storage of both cations and anions simultaneously in the same electrode materials, has been developed to enhance the volumetric/gravimetric capacity and the energy density compared to traditional systems that only store either anions or cations. Moreover, some previous reports have claimed that the cationic and anionic co-storage electrodes have better cycling stability and improved kinetics. For examples, a covalent organic polymer consisting of viologen and phenyl units has been proposed for the storage of Li^+ and ClO_4^- ions [33], and an organic framework composed of viologen and triamine-phenyl-triazine blocks has been tailored for Li^+/PF_6^- co-storage [34]. These cation/anion co-storage electrodes exhibited high specific capacity, along with rapid kinetics facilitated by coulombic interactions between cationic and anionic carriers in the covalent framework. However, there is currently rare precedents for the application of cationic and anionic co-storage strategy in small organic molecules, including aromatic imides.

Herein, we report the introduction of NPC units as N-substituents on both ends of naphthalene/benzene diimide to obtain DNPC-XDI (X = N, B). The NPC groups demonstrate the ability to undergo ultra-rapid electro-polymerization under an electric field and promote the cationic and anionic co-storage behavior. Specifically, the Poly(DNPC-XDI) (X = N, B) consists of *p*-type aromatic imides groups, aiming to accommodate anions (PF_6^-) at higher potential, and *n*-type Poly(carbazole) backbones, aiming to accommodate cations (Li^+). As a prime example, the resulted Poly(DNPC-NDI) cathode based on this anion-cation co-storage mechanism can deliver a high capacity as high as 359.2 mAh g^{-1} and a broad voltage plateau between 4.3–1.5 V. Remarkably, the Poly(DNPC-NDI) cathode exhibits virtually no capacity fade even after enduring an impressive 10,000 cycles under the stringent condition of ultrafast charging/discharging rate at 10 A g^{-1}. Quantum chemical computations verified the π-π stacking-free chain-like structures of Poly(DNPC-XDI) (X = N, B) and their lithiation products, as well as the energetically favourable lithiation process. To delve deeper into the underlying mechanisms, we carried out a comprehensive exploration and kinetic analysis through a series of systematic experiments. A key finding is that this molecular construction approach holds broad applicability to other redox-active small organics, thus presenting an alternative and promising strategy for developing easily processable, cost-effective, and high-performance sustainable secondary battery.

2. Results and discussion

The synthesis of DNPC-NDI and DNPC-BDI monomers was carried out by introducing two NPC peripheral groups onto the naphthalene diimide (NDI) molecule (Fig. 1**a** and **Fig. S1-S2**). To validate the successful synthesis of DNPC-NDI and DNPC-BDI monomers, various morphology and structure characterization techniques were performed (**Fig. S3-S8** and **Table S1-S3**). The introduction of two NPC groups as N-substituents on the NDI molecule effectively led to favourable physicochemical characteristics. As shown in Fig. 1**b** and **Fig. S9-S10**, the NPC peripheral groups significantly reduced the HOMO/LUMO gaps of DNPC-NDI (1.91 eV) and DNPC-BDI (2.03 eV) compared to those of pristine NDI (3.63 eV) and BDI (4.42 eV). This indicates significant enhancements in the redox reaction kinetics of the DNPC-XDI (X = N, B) monomers, in contrast to the unmodified XDI molecules. Furthermore, the DNPC-XDI (X = N, B) monomers exhibit a torsional structure, unlike the planar XDI system (X = N, B), which is conducive to facilitating efficient ion insertion and extraction [35].

To determine whether the lithiation process of Poly(DNPC-XDI) is energetically favorable, density functional theory (DFT) calculations were conducted to reveal the optimized structures of DNPC-XDI (X = N, B) oligomers and their lithiation products (**Table S5**). All the lithiation products derived from $(DNPC\text{-}BDI)_3$ and $(DNPC\text{-}NDI)_3$ oligomers show chain-like structures without π-π stacking. The periodic annealing molecular dynamics (MD) simulations without solvent molecules were also conducted with the low-energy structures shown in **Table S6**. Notably, π-π stackings were not favourable in the oligomers and their lithiation products simulated with solvent molecules, indicating that the existence of solvent molecules can suppress π-π stacking of the oligomers and the lithiation products.

In the typical in-situ electro-polymerization process (Fig. 1**c**), the NPC units first undergo an electro-oxidative reaction to form cation radical species that are highly active in coupling with each other, and then yield corresponding long-chain polymer. As shown in Fig. 1**d**, the initially pristine DNPC-NDI and DNPC-BDI electrodes exhibited dark orange colors, which turned to black after undergoing electro-polymerization and thus visually confirmed the successful preparation of Poly(DNPC-NDI) and Poly(DNPC-BDI). To further demonstrate the yield of Poly(DNPC-NDI) and Poly(DNPC-BDI), aattenuated total reflection-Fourier transform infrared (ATR-FTIR) spectra were collected (Fig. 1**e-f**). For the pristine DNPC-NDI and DNPC-BDI electrodes, the same peaks located at 746 cm^{-1} were both observed, which originated from the bi-substituted benzene rings [36]. In contrast, the products after electro-polymerization exhibited greatly wakened peaks of bi-substituted benzene rings and two newly emerged bands at around 774 and 834 cm^{-1}, which are ascribed to the tri-substituted benzene ring, demonstrating the formation of dimeric carbazoles in Poly(DNPC-NDI) and Poly(DNPC-BDI). Besides, we have conducted gel permeation chromatography (GPC) measurements to investigate the structure characteristics of Poly(DNPC-XDI) (X = N, B). Due to the low solubility of the electro-polymerization product, only Poly(DNPC-XDI) with low polymerization degree could dissolve into tetrahydrofuran (THF) and then being detected by GPC methods. As shown in **Fig. S11**, the GPC results of Poly(DNPC-NDI) and Poly(DNPC-BDI) delivered a molecular weight of 2284 and 2187 g mol^{-1}, respectively, These results demonstrate the successful polymerization of DNPC-NDI and DNPC-BDI monomers and indicate the polymerization degree of these two in-situ electro-polymerization products are at least 3. Besides, we have converted the GPC traces from elution time to Log(M_W). As shown in **Fig. S11c-d,** it is evident that neither DNCP-NDI nor DNCP-BDI monomers are detected. The close proximity of the number-average molecular weight (M_n) and weight-average molecular weight (M_w) for Poly(DNCP-NDI) indicates a predominant trimeric structure, while the relatively lower M_n of Poly(DNCP-BDI) suggests the coexistence of dimer, trimer, and tetramer. Given the absence of direct signals indicative of long-chain polymers, it is necessary to clarify that the in-situ polymerized

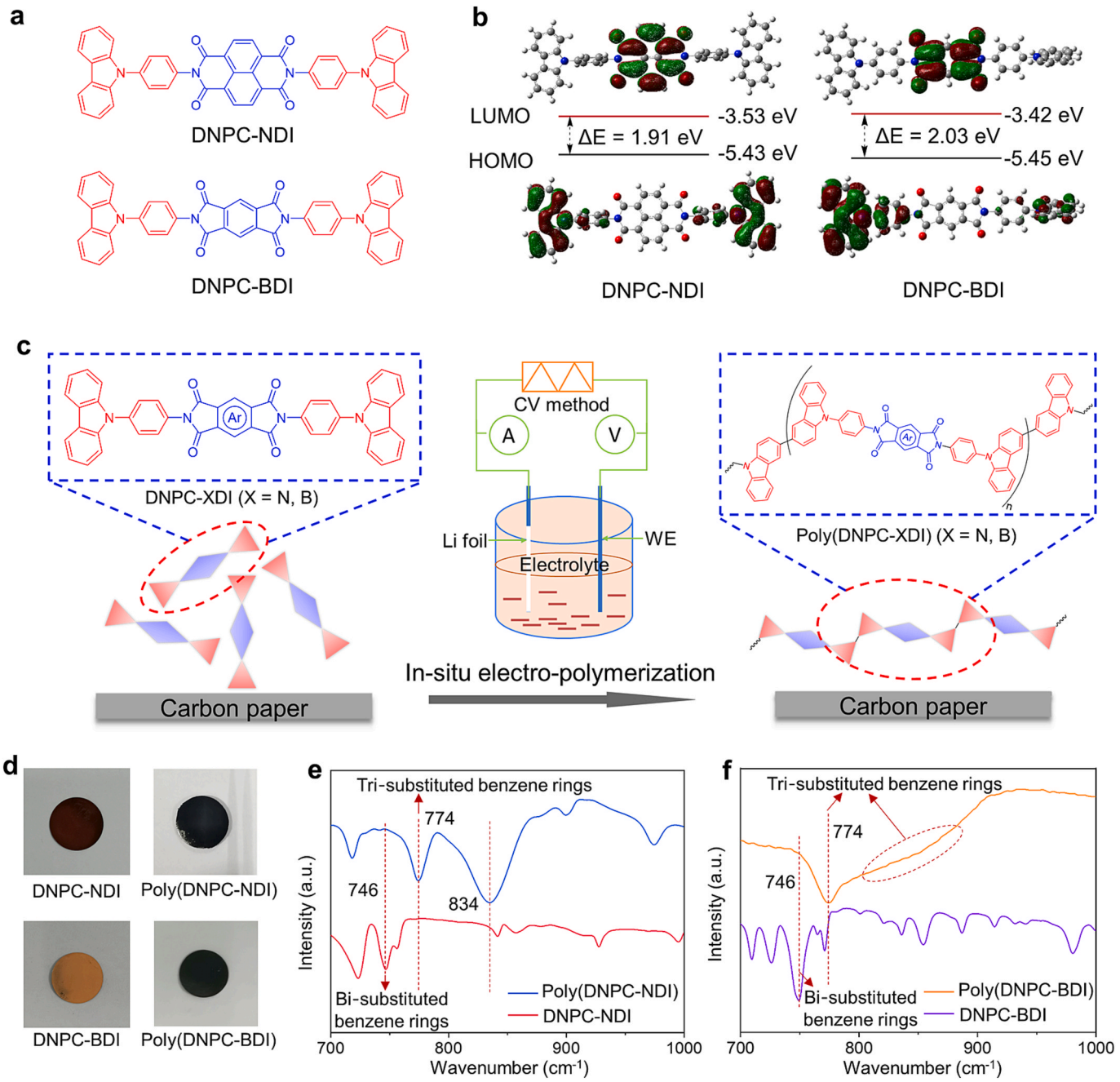

Fig. 1. (a) Molecule structure of DNPC-NDI and DNPC-BDI. (b) DFT calculated HOMO and LUMO energy levels of DNPC-NDI and DNPC-BDI, where the HOMO–LUMO energy gaps are presented. (c) Illustration of in-situ electro-polymerization process of DNPC-XDI (X = N, B). (d) Digital photographs of DNPC-NDI and DNPC-BDI electrodes before and after the electro-polymerization. (e, f) ATR-FTIR spectra of (e) DNPC-NDI and (f) DNPC-BDI electrodes before and after the electro-polymerization, respectively.

Poly(DNCP-XDI) in this study is more likely to exist in the form of oligomers. The low solubility of the long-chain Poly(DNCP-XDI) is primarily due to the extended π-conjugation in the DNCP-XDI monomers, which becomes even more pronounced in the Poly(DNCP-XDI), further reducing its solubility. Consequently, the actual degree of polymerization (DP) of the in situ polymerized Poly(DNPC-XDI) (X = N, B) in the cathode is expected to be substantially higher than the measured values.

The electrochemical performances of Poly(DNPC-NDI) and Poly (DNPC-BDI) electrodes were measured in coin cells using lithium foil as the counter electrode and a solution of 1 M $LiPF_6$ in ethylene carbonate/diethyl carbonate electrolyte (EC/DEC, 1:1 by volume). CV tests were carried out at a scan rate of 0.5 mV s^{-1} within a potential range of 1.5–4.3 V *vs.* Li/Li^+ to elucidate the $Li+/PF_6^-$ storage behaviors. As shown in Fig. 2**a**, the initial scan of Poly(DNPC-NDI) showed two pairs of reversible redox waves at 2.32/2.10 V and 2.41/2.56 V, which was attributed to the Li^+ loading/detaching behaviors of carbonyl groups, respectively. These two couples of peaks were replaced by single broad peaks at about 2.36/2.52 V in the 3rd consecutive cycle, which are related to the structural changes during the electro-polymerization process. During the first scan, in the high-voltage region, there was an oxidative peak located at 4.13 V and two reductive peaks appeared at 3.88 and 4.11 V, respectively. The former peak was assignable to the formation of the dicarbazole radical cations with the doping of anions (PF_6^-), and the latter corresponded to the reduction of dimeric carbazole dications to its neutral states via stepwise two-electron processes accompanied by the dedoping of PF_6^-. Besides, there was an additional

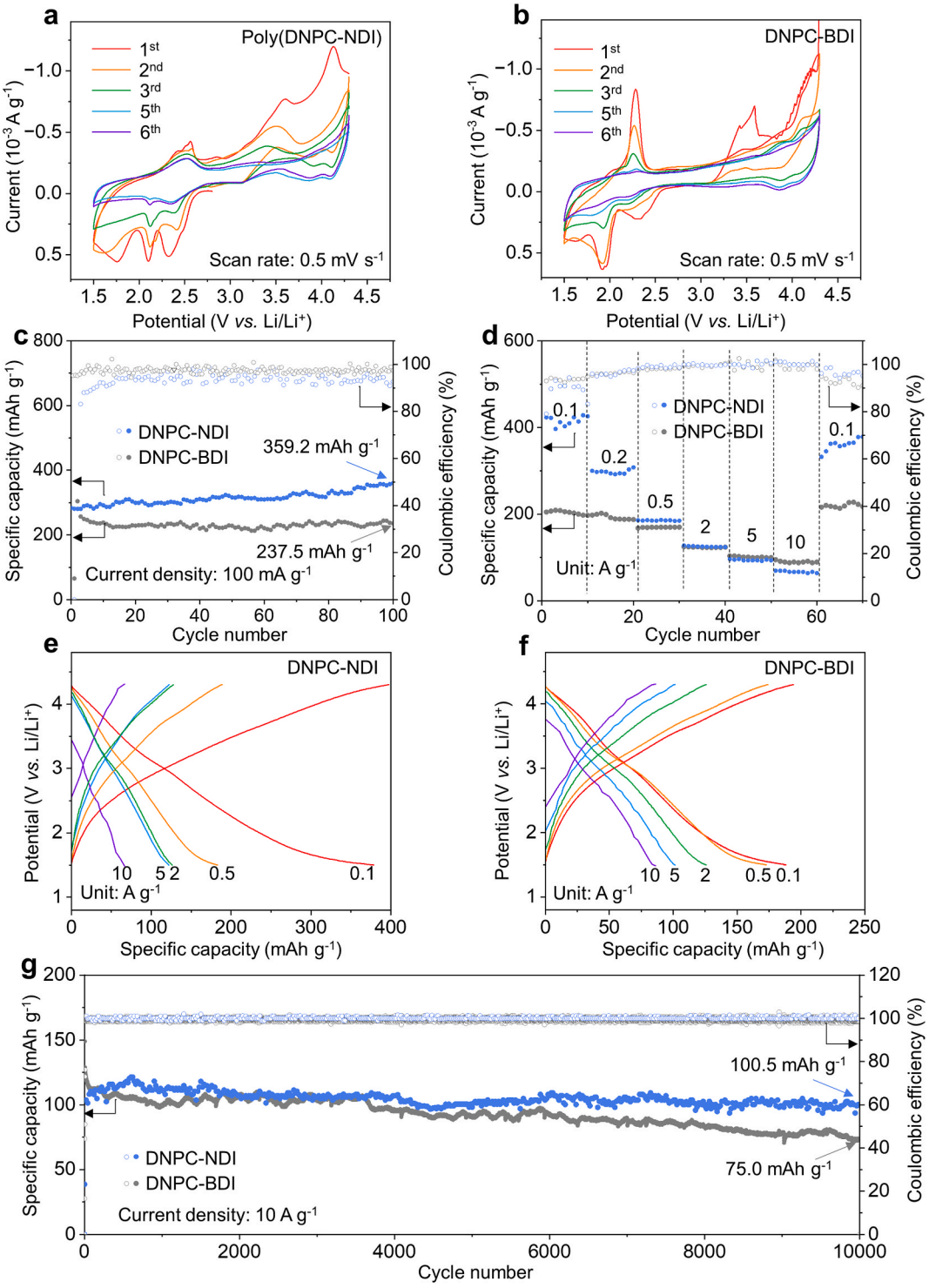

Fig. 2. (a, b) CV curves for the conversion processes (a) from DNPC-NDI to Poly(DNPC-NDI) and (b) from DNPC-BDI to Poly(DNPC-BDI) at a scan rate of 0.5 mV s^{-1} within the voltage range of 1.5–4.3 V *vs.* Li/Li^+, respectively. (c) Cycling performances and Coulombic efficiencies of Poly(DNPC-NDI) and Poly(DNPC-BDI) electrodes tested at a current density of 100 mA g^{-1}. (d) Rate capabilities of Poly(DNPC-NDI) and Poly(DNPC-BDI) electrodes at the current densities from 0.1 to 10 A g^{-1}. (e, f) Galvanostatic discharge/charge profiles of (e) Poly(DNPC-NDI) and (f) Poly(DNPC-BDI) electrodes at various current densities, respectively. (g) Long-term cycling performances of Poly(DNPC-NDI) and Poly(DNPC-BDI) electrodes at 10 A g^{-1}.

pair of peaks observed at 3.46 and 2.46 V, indicative of charge trapping, which is owing to the confinement of mobile charges in the polymer matrix through defects or other effects [36]. The CV curves of the Poly (DNPC-BDI) cathode were also depicted in Fig. 2**b**; Similarly, there was one oxidative peak positioned at 2.28 V and two reductive peaks located at 2.27 and 1.92 V, which were attributed to the Li^+ uptake/detachment onto/from the carbonyl groups. In the high-voltage region, there was also an obvious doping/de-doping behavior involving an oxidative peak that appeared at 4.12 V and two redox waves located at 4.08 and 3.86 V on the return cycle assigned to the first and second reductions of the $[bis\text{-}carbazole]^{2+}$ units.

Notably, both the CV curves of Poly(DNPC-NDI) and Poly(DNPC-

BDI) electrodes at high-voltage region exhibited the typical 4-electron ECCE (where "E" represents electron transfer, "C" represents chemical) process in indole-containing compounds [35–39], resulting in the dimerization via aryl-aryl coupling and further sequential polymerization of the DNPC-XDI (X= N, B) monomers. Specifically, from Fig. S12, the carbazole units in the unit of DNPC-XDI (X= N, B) first lost one electron to form carbazole radical cations under the influence of an electric field. Then, two carbazole radical cations coupled and underwent double deprotonation to rearomatize and finally form the dimerization product. Oxidation of dimerization product generates new radical cations that further react with monomer radical cations or dimer radical cations to form trimers or tetramers, hence resulting in stepwise chain elongation and forming the final in-situ electro-polymerization products, e.g. Poly(DNPC-NDI) or Poly(DNPC-BDI). Above all, the carbonyl groups within this polymer acted as redox sites via the reversible binding and detaching of Li^+ ions, while the carbazole groups served as both polymerization agents and redox-active sites via doping and de-doping mechanisms.

Furthermore, electrochemical impedance spectroscopy (EIS) of the batteries before and after the in-situ electro-polymerization process were compared. In Fig. S13, the semicircle radius in the high-frequency region of the battery after in-situ electro-polymerization (66.3 O) was much smaller than that of the pristine state (35.5 O), suggesting the sharply decreased charge transfer resistance at the electrode–electrolyte interface after the electro-polymerization process, which remarkably facilitated fast ion transport and benefited rate performance.

The electrochemical performances of Poly(DNPC-NDI) and Poly (DNPC-BDI) electrodes were systematically measured (Fig. 2**c-g**). The Poly(DNPC-NDI) cathode delivered an initial discharge capacity of 310.0 mAh g^{-1}, with an initial Coulombic efficiency of 95.3 % (Fig. 2**c**). After 100 cycles, the discharge capacity could be maintained at 359.2 mAh g^{-1}. In contrast, the Poly(DNPC-BDI) cathode exhibited an initial discharge capacity of 256.5 mAh g^{-1} with a Coulombic efficiency of ~ 97.8 % and kept at 238.3 mAh g^{-1} after 100 cycles. The rate performances were also measured at progressively increased current densities ranging from 0.1 to 10 A g^{-1} (Fig. 2**d**). The Poly(DNPC-NDI) cathode exhibited high discharge capacities of 424.0, 301.5, 185.4, 124.3, 96.4 and 70.0 mAh g^{-1}, with high Coulombic efficiencies of 94.5, 96.2, 98.7, 99.8, 99.9 and 100.1 % at 0.1, 0.2, 0.5, 2.0, 5.0 and 10 A g^{-1}, respectively. The specific capacity was restored to 376.8 mAh g^{-1} when the current density returned to 0.1 A g^{-1}. The Poly(DNPC-BDI) cathode based on cation–anion co-storage mechanism exhibited specific discharge capacity of 238.1, 189.5, 170.7, 125.9, 102.7 and 91.7 mAh g^{-1} and Coulombic efficiencies of 93.6, 96.3, 98.8, 99.3, 99.7 and 99.8 % at 0.1, 0.2, 0.5, 2.0, 5.0 and 10 A g^{-1}, respectively. The charge–discharge curves at various current densities (Fig. 2**e,f**) displayed an inconspicuous plateau behavior of Poly(DNPC-NDI) and Poly(DNPC-BDI) cathodes. All the charge/discharge voltage profiles exhibit one discharge plateau at about 3.0 V and one slightly sloping charge plateau, suggesting that both the Poly(DNPC-NDI) and Poly(DNPC-BDI) electrodes work well at high rates. The long-term cycling performances of Poly(DNPC-NDI) and Poly(DNPC-BDI) were tested at an ultrahigh rate of 10 A g^{-1}. In Fig. 2**g**, the Poly(DNPC-NDI) cathode showed an initial discharge capacity of 109.5 mAh g^{-1} with Coulombic efficiencies kept at above 99.5 %. Subsequently, the discharge capacity remained ultrastable and still maintained 100.5 mAh g^{-1} after 10,000 cycles, representing one of the most remarkable cycling stabilities among the reported organic cathode materials. Meanwhile, the Poly(DNPC-BDI) cathode initially delivered a discharge capacity of 118.4 mAh g^{-1} and maintained 75.0 mAh g^{-1} after 10,000 cycles, demonstrating an average capacity decay of only 0.0036 % per cycle. We have measured the electrochemical performances of the Poly(DNPC-NDI) and Poly(DNPC-BDI) electrodes with a high areal mass loading of 9.9 and 8.3 mg cm^{-2}, respectively. As shown in Fig. S14, the Poly(DNPC-NDI) cathode achieved a discharge capacity of 92.9 mAh g^{-1} with an initial Coulombic efficiency of 99.9 % after 100 cycles (Fig. S14**a**). Analogously, the Poly (DNPC-BDI) cathode exhibited a discharge capacity of 118.9 mAh g^{-1} with a Coulombic efficiency of ~ 100.5 % after 100 cycles. The decreased capacity utilization ratio is attributed to relatively limited amounts of the electrolyte when assembled with the electrode with high mass loading.

For comparison, the unmodified NDI and BDI electrodes, as control samples, showed poor electrochemical properties with low capacity, unpromising rate performance, and poor cycling stability (Fig. S15-S16). These results suggest that by harnessing the intrinsic conductivity and insolubility of the Poly(carbazole) skeleton along with the redox activity of both carbazole backbone and aromatic imide groups, the Poly (DNPC-XDI) (X = N, B) achieved outstanding electrochemical performance including high capacity, excellent rate performance, and impressive cycling stability. To investigate the solubility of Poly(DNPC-XDI) (X = N, B) electrodes, we have conducted UV–Vis characterizations of the electrodes in the initial state, under different charging/discharging states, and after high-current cycling (Fig. S17). Specifically, we disassembled the coin cells at various charge/discharge states and after cycling 1000 cycles at 10.0 A g^{-1}, and then soaked these electrodes into DC/DEC (1:1 by volume) solution for 24 h. After that, we measured the UV–Vis spectra on the supernatant of each sample (inset of Fig. S17 **a-b**) to analyze the solubility of Poly(DNPC-XDI) under different charging/discharging states, and after high-current cycling. As a result, in the UV–Vis spectrum of pristine DNPC-XDI (X = N, B) electrodes, the strong absorption peaks at ~ 238, ~288, and ~ 333 nm are attributed to the n → π* transition of the carbonyl group, $A_{1g} \rightarrow B_{2u}$ and $A_{1g} \rightarrow B_{1u}$ transition of the benzene ring, and intramolecular charge-transfer absorption, respectively [40]. In contrast, after in situ electro-polymerization, the UV–Vis spectra of all the as-prepared Poly(DNPC-XDI) (X = N, B) electrodes did not exhibit the characteristic peaks, indicating their low solubility under different charging/discharging states and after high-current cycling. Besides, the relatively strong absorption peaks at about 212 nm is associated with the residual EC/DEC solvent remained on the as-prepared electrodes [41]. We also collected the SEM images of Poly(DNPC-XDI) (X = N, B) cathodes before and after in-situ electro-polymerization, and cycling after 1000 cycles at a high rate of 10 A g^{-1}. From Fig. S18-**19**, it is shown that the surface morphology of Poly (DNPC-XDI) (X = N, B) electrodes transformed from dense stacked layers to micro-nano scale particles after in situ electro-polymerization, and this dense structure can be well maintained even in 1000th cycles at 10 A g^{-1}. This results demonstrate the good structural stability of the Poly(DNPC-XDI) (X = N, B) cathodes during the cycling process.

The reaction kinetics and Li-ion diffusivity of Poly(DNPC-NDI) and Poly(DNPC-BDI) electrodes were evaluated by CV scans at different rates (Fig. 3**a-b**). The contributions of capacitive and diffusion processes can be quantified according to the following equations: [42].

$$i(V) = k_1\nu + k_2\nu^{1/2} \quad (1)$$

$$i(V)\ \nu^{-1/2} = k_1\nu^{1/2} + k_2 \quad (2)$$

where $k_1\nu$ and $k_2\nu^{1/2}$ stand for the fraction of the capacitive and diffusion effects, respectively. As shown in Fig. 3**c**, for Poly(DNPC-NDI) cathode, the pseudocapacitive storage fraction of the total capacity was 45 %, 62 %, and 65 % at a scan rate of 0.5, 1.5, and 2.0 mV s^{-1}, respectively. For Poly(DNPC-BDI) cathode, the contribution ratios of the capacitive process at scan rates of 0.1, 1.0, 0.5, and 1.5 mV s^{-1} were 51 %, 58 %, 63 %, and 67 %, respectively. Compared with the Poly(DNPC-BDI) electrode, the Poly(DNPC-NDI) cathode demonstrated a higher capacity, which may be partially attributed to the lower HOMO/LUMO gap of DNPC-NDI (1.91 eV) compared to that of DNPC-BDI (2.03 eV). Additionally, DFT calculations indicate that the binding energies of Li^+ ions with $(DNPC\text{-}NDI)_3$ oligomers are greater than those with $(DNPC\text{-}BDI)_3$ oligomers, suggesting that Li^+ ions can more readily bind with $(DNPC\text{-}NDI)_3$. Consequently, the enhanced capacity of the Poly(DNPC-NDI) cathode is likely associated with its higher conductivity and stronger binding capability with Li^+, similar to the previous literature [43]. Fig. 3**d** displayed the plots of the potential (V) versus the b-value. The b-values obey the following power law given equation: [44].

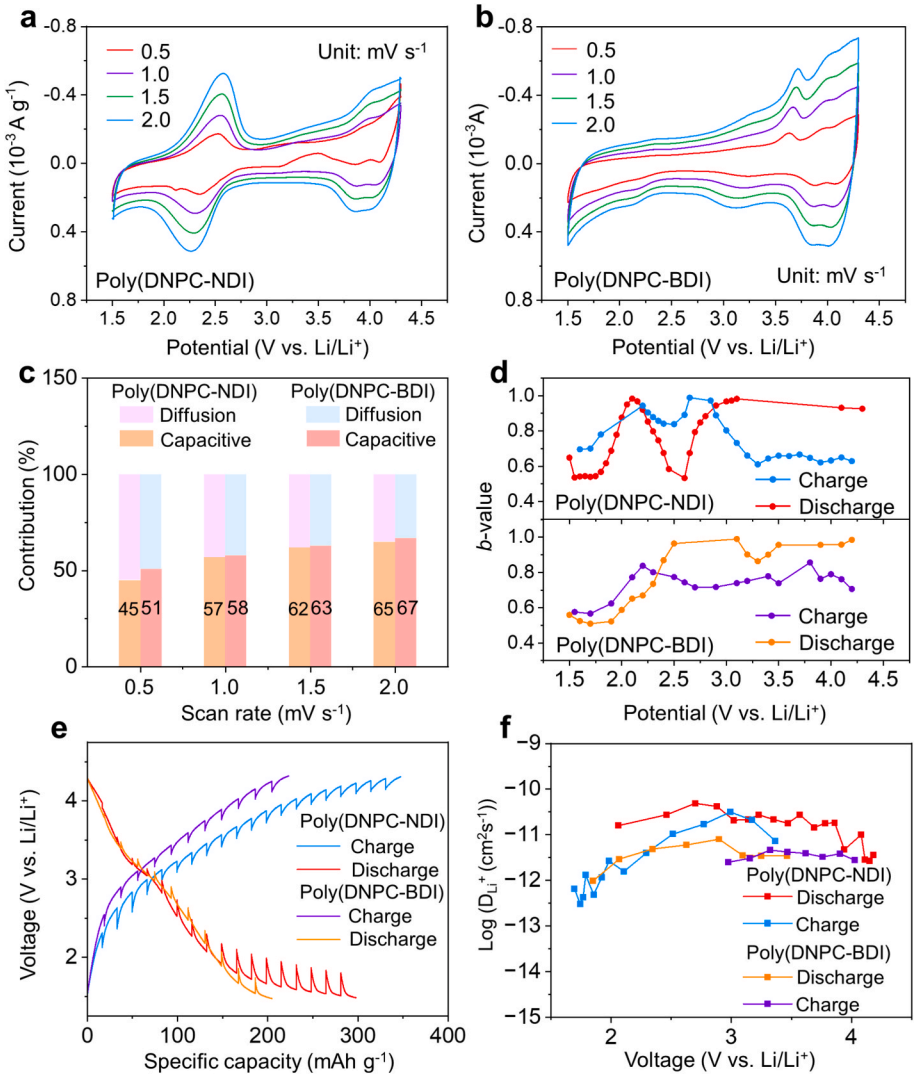

Fig. 3. CV curves of (a) Poly(DNPC-NDI) and (b) Poly(DNPC-BDI) electrodes at different scan rates. (c) Normalized contribution ratios of capacitive capacities and diffusion-controlled capacities of Poly(DNPC-NDI) and Poly(DNPC-BDI) electrodes at different scan rates. (d) Calculated b-values as a function of potential for the discharged and charged sweeps in Poly(DNPC-NDI) and Poly(DNPC-BDI) electrodes. (e) Potential responses of Poly(DNPC-NDI) and Poly(DNPC-BDI) electrodes during GITT measurements at a constant current density of 200 mA g^{-1} and (f) corresponding ion diffusion coefficients calculated from the GITT results.

$i(V) = a\nu^b$ (3)

$\lg i(V) = b\lg\nu + \lg a$ (4)

where the slope of the linear fit of the log–log plot corresponds to b. A value near unity (b = 1) indicates fully surface-controlled processes while b = 0.5 implies purely diffusion-controlled processes, respectively. As for Poly(DNPC-NDI) cathode, during the discharged/charged processes, the b values showed similar manifestation, that is, the minimum values both appeared at 2.5 V, which corresponded to the diffusion-controlled behavior associated with the Li^+ loading/detaching on carbonyl groups. Over 2.5 V, the b values at discharged states were near 1.0, indicating purely capacitive-controlled processes, this behavior aligns with the de-doping of PF_6^- ions and the subsequent formation of an extended π-conjugated structure at this region. Conversely, during the charged process, the b values decreased and maintained at about 0.6, this suggests a limitation in pseudocapacitive behavior, likely induced by the presence of highly doped PF_6^- ions, which disrupt the inherent conjugated system of Poly(DNPC-NDI). As for Poly(DNPC-BDI) cathode, when the potential was below 2.5 V in both discharged/charged processes, the b values were in a range of 0.5–0.8, revealing the confusion-controlled behavior associated with the Li^+ loading/detaching processes on carbonyl groups. Over 2.5 V, the b values at discharged states were near to 1.0, indicating purely capacitive-controlled processes, corresponding to the PF_6^- de-doped behaviors and subsequently formed the long-range π-conjugated structure.

Moreover, galvanostatic intermittent titration technique (GITT) measurements were conducted to analyze the ion diffusion coefficients (D_{ion}), as presented in Fig. 3**e**. The ion diffusion coefficients for Poly (DNPC-NDI) and Poly(DNPC-BDI) cathodes were calculated to be between 10^{-13} to 10^{-11} cm^2 s^{-1} during the discharge–charge cycles (Fig. 3**f**), indicating good ion conductivity compared with the parallel studies [5,45–46].

To investigate the charge storage mechanism of Poly(DNPC-XDI), we conducted ex-situ X-ray photoelectron spectroscopy (XPS), scanning electron microscopy (SEM), and energy-dispersive X-ray spectroscopy (EDX) on Poly(DNPC-NDI) electrode at different charged/discharged states. The XPS spectra at the F 1s region of Poly(DNPC-NDI) electrode at fully-charged/discharged states showed three deconvoluted peaks at 1388.7 eV, 1685.1 eV, and 1792.3 eV, which can be ascribed to C–F, N–PF_6^- and Li–PF_6^- bonds, respectively (Fig. 4**a-b**). At fully-charged state, the N–PF_6^- signal sharply strengthened with the significant decrease of Li–PF_6^- content, indicating the doping of PF_6^- from the

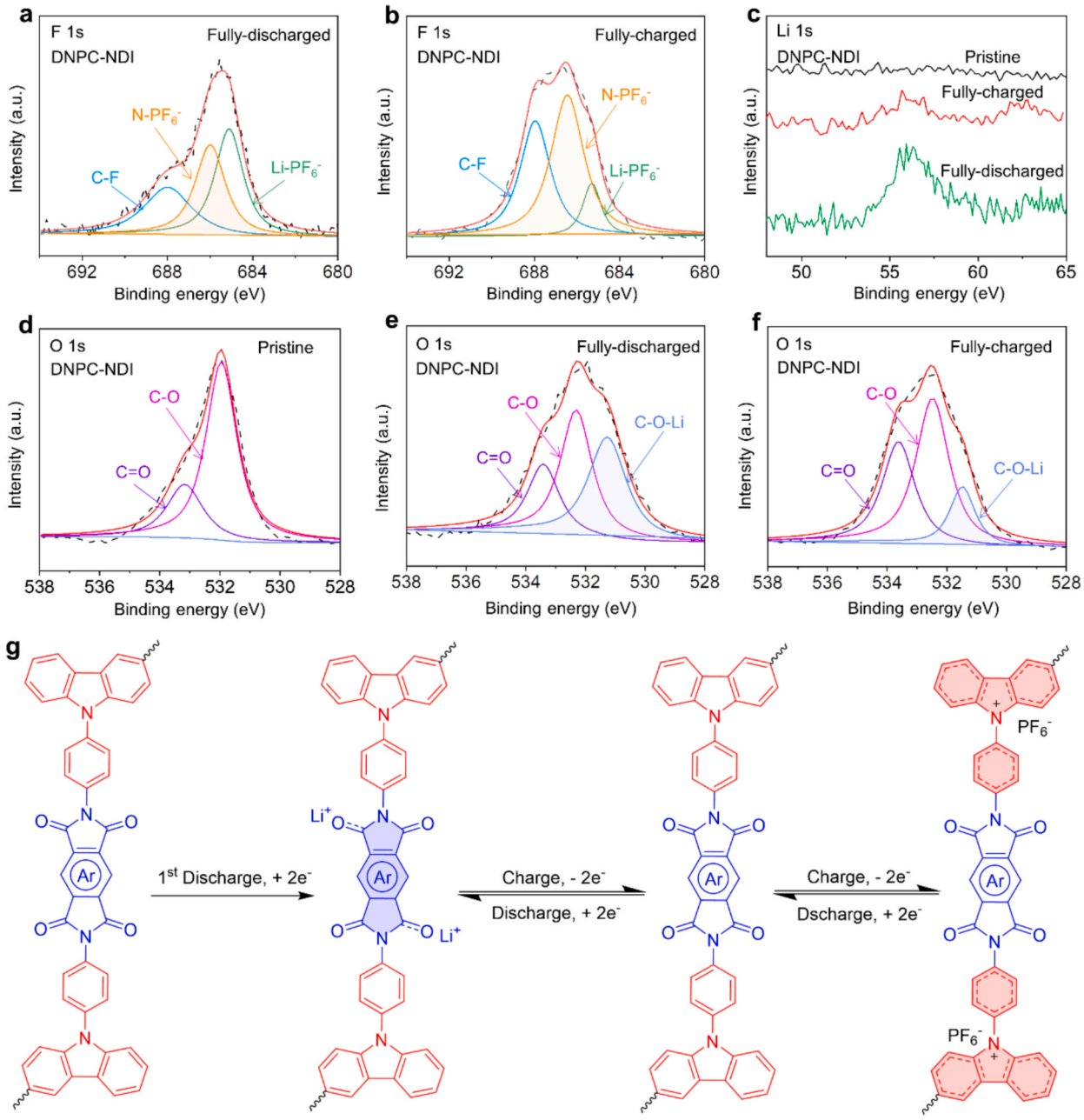

Fig. 4. (a, b) XPS spectra at F 1s region of Poly(DNPC-NDI) electrode at (a) fully-discharged and (b) fully-charged states, respectively. (c) XPS spectra at Li 1s region of Poly(DNPC-NDI) electrode at denoted states. (d) XPS spectra at the O 1s region of Poly(DNPC-NDI) electrode were measured at (d) pristine, (e) fully-discharged, and (f) fully-charged states, respectively. (g) Schematic illustration of the cationic and anionic co-storage mechanism of Poly(DNPC-XDI) (X = N, B) electrodes.

electrolyte into the Poly(DNPC-NDI) electrode. Reversibly, the content of N–PF_6^- at fully-charged state decreased compared to the fully-charged state, corresponding to the de-doping of PF_6^- from the Poly-carbazole skeleton. Notably, there were still a considerable number of N–PF_6^- bonds left due to the partial remaining PF_6^- anions in the polymer system that compensated for the charge imbalance caused by electro-polymerization. Ex-situ EDX results (**Fig. S20a-b**) also showed that the atomic ratios of the Poly(DNPC-NDI) electrode at fully-discharged and fully-charged states were 0.148 and 0.246, respectively, indicating the reversible PF_6^- doping/de-doping into/from the Poly(DNPC-NDI) during the charged/discharged processes. Moreover, the high-resolution XPS spectrum at the O 1s region of the Poly(DNPC-NDI) electrode was deconvoluted into three peaks attributed to C=O (533.2 eV) and C–O (531.9 eV), as shown in Fig. 4**d**. While discharging to 1.5 V, there was a new peak emerging at 531.3 eV assigned to C–O–Li bonds, revealing the interaction of Li^+ with C=O bonds during the lithiation process. Subsequently, when fully charged to 4.3 V (Fig. 4**f**), the signal intensities of C–O–Li species became weaker while the peaks of C=O bonds got stronger, suggesting the conversion from C–O–Li to C=O during the charge processes. As shown in Fig. 4**c**, the intensities of Li 1s signals increased at the fully discharged state and deceased during the charge processes, suggesting the reversible Li^+ insertion/extraction into/from Poly(DNPC-NDI) cathode. Besides, as for the ratio of C=O to C-O in the fully charged state is not consistent with the ratio in the initial state, this is because the lithium interaction/de-interaction occurred in this system is not completely thorough, which is consistent with the appearance of Li 1s XPS with little intensity in the fully charged state. Moreover, ex-situ SEM measurements (**Fig. S21a-d**) revealed that the Poly(DNPC-NDI) electrode had no obvious morphological change at different charging states.

The Li-storage mechanism was further characterized by ex-situ FT-IR spectroscopy (Fig. S22). The stretching vibration peaks of C=O in the pristine DNPC-NDI and DNPC-BDI cathodes were observed at 1666 cm^{-1} and 1697 cm^{-1}, respectively. During the discharge process, the intensity of the C=O peaks decreased due to interactions with Li^+ ions, and these peaks were partially restored upon charging to 4.3 V. The incomplete disappearance of the C=O peaks is attributed to the presence of inactive carbonyl groups within the imide active structure. Additionally, when compared with the pristine DNPC-XDI (X = N, B) electrode, the characteristic peak of PF_6^- anions at 835 cm^{-1} was obviously enhanced after full charging, indicating the doping process between PF_6^- anions with the nitrogen atoms in the carbazole backbone during the charging process.

Based on the above analyses, it is concluded that the charge storage mechanism of Poly(DNPC-XDI) (X = N, B) electrodes were based on a typical loading/detaching behavior of Li^+ cations on redox-active imide carbonyl groups and a capacitive process that depends on doping/dedoping of PF_6^- anions on Poly-carbazole backbone. As illustrated in Fig. 4**g**, in a typical discharge–charge process, when the battery is discharged to ~3.5 V, the imide C=O groups gain electrons to be reduced to imide C–O^-, which could interact with Li^+ cations in the electrolyte. When fully discharging to ~1.5 V, the PF_6^- anions would be removed from the doped Poly-carbazole skeletons. Reversibly, when the battery subsequently charged to 2.5 V, the imide C–O^- bonds were firstly oxidized to imide C=O, accompanied by the detaching of Li^+ cations from aromatic imide groups. When further charged to 4.3 V, the Poly-carbazole backbones recovered the anion-doped states through the re-interaction with PF_6^- anions in the electrolyte.

We further performed density functional theory (DFT) study to explore the thermodynamic properties and molecular structure variations during the lithiation process. The low-energy structures of lithiation products derived from $(DNPC\text{-}XDI)_3$ (X = N, B) and the binding energies of Li^+ ions with $(DNPC\text{-}XDI)_3$ (X = N, B) were calculated by DFT calculations (Fig. 5). The binding energies of Li^+ ions with $(DNPC\text{-}XDI)_3$ gradually become higher with the increase of attached Li^+ ions, indicating that the lithiation of $(DNPC\text{-}XDI)_3$ oligomers is energetically favorable. Besides, the binding energies of Li^+ ions with $(DNPC\text{-}NDI)_3$ oligomer are larger than that with $(DNPC\text{-}BDI)_3$, suggesting that Li^+ can more easily bind with $(DNPC\text{-}NDI)_3$. These calculation results are qualitatively consistent with the above experimental results.

3. Conclusion

In this study, we present a promising molecular engineering strategy for structure regulation and in-situ polymerization of redox-active small organics to realize simultaneous co-storage of Li^+ cations and PF_6^- anions. Specifically, we symmetrically introduced NPC units as N-substituent side groups onto aromatic imides to obtain DNPC-XDI (X = N, B). The strategic grafting of two NPC groups facilitates the in-situ electropolymerization process of aromatic imide monomers, achieving a controlled degree of polymerization 2–4. This molecular design

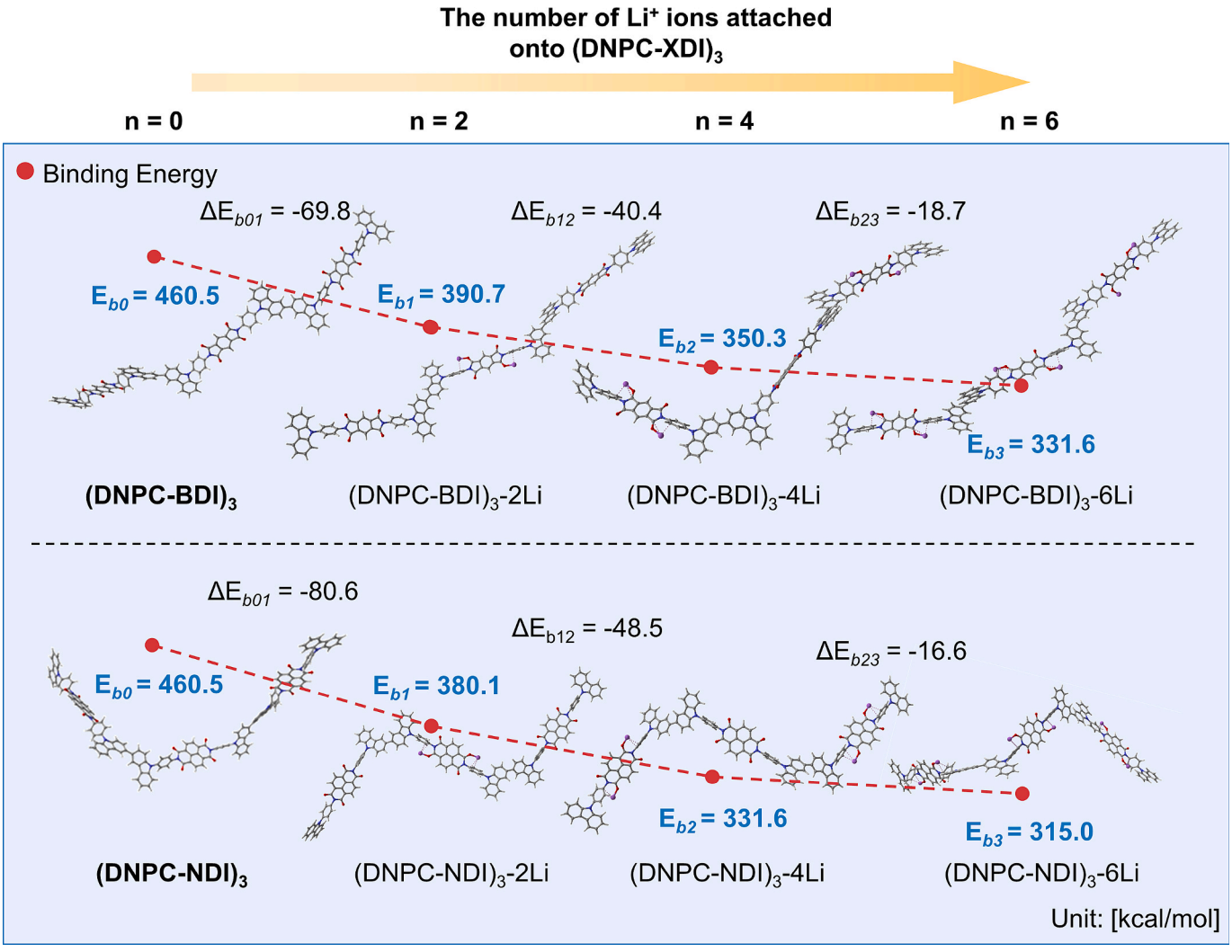

Fig. 5. Low-energy structures of lithiation products derived from $(DNPC\text{-}XDI)_3$ (X = N, B) and the binding energies of Li ions with $(DNPC\text{-}XDI)_3$.

simultaneously introduces abundant anion storage sites, and also enhances the overall electrochemical properties. Benefiting from the newly-involved p-type charge storage mechanism with high thermodynamic insertion potentials, the resultant Poly(DNPC-XDI) cathodes exhibit ultrahigh cut-off voltage (4.3 V), high capacity, high rate capability, and unprecedented cycling stability. The charge storage behaviors of Poly(DNPC-XDI) were systematically investigated via ex-situ XPS, EDX, and SEM measurements. We revealed that the charge storage mechanism of Poly(DNPC-XDI) involves a loading/detaching process of Li^+ cations on carbonyl groups via C=O/C-O$^-$ transformation and a doping/de-doping process of PF_6^- anions on Poly(carbazole) backbones, which can also be evidenced by theoretical calculations. Electrochemical kinetics analyses indicated that both the diffusion process and pseudocapacitive process contribute to the charge storage capacity of the Poly(DNPC-XDI) electrodes. Notably, this innovative molecular engineering strategy could be extended to other redox-active organic/polymer systems, thus providing a promising avenue for developing high-performance, cost-competitive, and easy-to-process organic/polymer electrode materials for practical and sustainable secondary batteries.

CRediT authorship contribution statement

Xinmei Song: Formal analysis, Data curation, Conceptualization. **Qianchuan Yu:** Methodology, Investigation. **Junjie Li:** Funding acquisition, Formal analysis. **Zuoao Wu:** Project administration, Investigation. **Yizhi Xing:** Software, Investigation. **Yaoda Wang:** Software, Project administration. **Lina Qin:** Software, Funding acquisition. **Huapeng Sun:** Methodology. **Zuoxiu Tie:** Visualization, Validation, Software. **Jing Ma:** Validation, Supervision, Software. **Zhong Jin:** Writing – original draft, Supervision, Conceptualization.

Declaration of competing interest

The authors declare that they have no known competing financial interests or personal relationships that could have appeared to influence the work reported in this paper.

Acknowledgments

The authors appreciate the financial support from the National Natural Science Foundation of China (22479074 and 22475096), the General Project of the Joint Fund of Equipment Pre-research and the Ministry of Education (8091B02052407), the Natural Science Foundation of Jiangsu Province (BK20240400 and BK20241236), the Science and Technology Major Project of Jiangsu Province (BG2024013), the Scientific and Technological Achievements Transformation Special Fund of Jiangsu Province (BA2023037), the Academic Degree and Postgraduate Education Reform Project of Jiangsu Province (JGKT24_C001), the Key Core Technology Open Competition Project of Suzhou City (SYG2024122), the open research fund of Suzhou Laboratory (SZLAB-1308-2024-TS005), the Gusu Leading Talent Program of Scientific and Technological Innovation and Entrepreneurship of Wujiang District in Suzhou City (ZXL2021273), and the Chenzhou National Sustainable Development Agenda Innovation Demonstration Zone Provincial Special Project (2023sfq11). All calculations in this work were performed with computational resources on an IBM Blade cluster system in the High Performance Computing Center (HPCC) of Nanjing University.

Author contributions

Z. J. conceived the idea of this study. X. S. and Q. Y. performed the preparation of materials. J. L. and J. M. contributed to the DFT calculations. X. S. and L. Q. performed the XRD, Raman, and XPS analyses. X. S. performed the electrochemical measurements. X. S., H. S., Z. T., and J. M. contributed to the data analysis. Z. J. and X. S. analyzed the data and wrote the paper. Z. J. revised the manuscript and supervised the project. All authors discussed the results and commented on the manuscript.

Appendix A. Supplementary data

Supplementary data to this article can be found online at https://doi.org/10.1016/j.cej.2025.162419.

Data availability

Data will be made available on request.

References

[1] M. Bhosale, S. Chae, M. Kim, J. Choi, Organic small molecules and polymers as an electrode material for rechargeable lithium-ion batteries, *J. Mater. Chem. A* 6 (2018) 19885–19911, https://doi.org/10.1039/c8ta04906h.
[2] D. Deng, Li-ion batteries: basics, progress, and challenges, *Energy Sci. Eng.* 3 (2015) 385–418, https://doi.org/10.1002/ese3.95.
[3] M. Palacin, Recent advances in rechargeable battery materials: a chemist's perspective, *Chem. Soc. Rev.* 38 (2009) 2565–2575, https://doi.org/10.1039/b820555h.
[4] J. Tarascon, M. Armand, Issues and challenges facing rechargeable lithium batteries, *Nature* 414 (2001) 359–367, https://doi.org/10.1038/35104644.
[5] X. Deng, J. Li, L. Ma, J. Sha, N. Zhao, Three-dimensional porous carbon materials and their composites as electrodes for electrochemical energy storage systems, *Mater. Chem. Front.* 3 (2019) 2221–2245, https://doi.org/10.1039/c9qm00425d.
[6] J. Li, Q. Xu, G. Li, Y. Yin, L. Wan, Y. Guo, Research progress regarding Si-based anode materials towards practical application in high energy density Li-ion batteries, *Mater. Chem. Front.* 1 (2017) 1691–1708, https://doi.org/10.1039/c6qm00302h.
[7] L. Li, Y. Yin, J. Hei, X. Wan, M. Li, Y. Cui, Molecular engineering of aromatic imides for organic secondary batteries, *Small* 17 (2021) 2005752, https://doi.org/10.1002/smll.202005752.
[8] Y. Liang, Z. Tao, J. Chen, Organic electrode materials for rechargeable lithium batteries, *Adv. Energy Mater.* 2 (2012) 742–769, https://doi.org/10.1002/aenm.201100795.
[9] Y. Lu, J. Chen, Prospects of organic electrode materials for practical lithium batteries, *Nat. Rev. Chem.* 4 (2020) 127–142, https://doi.org/10.1038/s41570-020-0160-9.
[10] C. Li, A. Yu, X. Chen, T. He, S. Mei, G. Long, C. Yao, Dual-active centers of porous triazine frameworks for efficient Li storage, *Chem. Eng. J.* 489 (2024) 151103, https://doi.org/10.1016/j.cej.2024.151103.
[11] F. Huang, W. Zhao, Y. Guo, Y. Mi, S. Gull, G. Long, P. Du, Conjugated enhanced polyimide enables high-capacity ammonium ion storage, *Adv. Funct. Mater.* 34 (2024) 2407313, https://doi.org/10.1002/adfm.202407313.
[12] T. Schon, B. McAllister, P. Li, D. Seferos, The rise of organic electrode materials for energy storage, *Chem. Soc. Rev.* 45 (2016) 6345–6404, https://doi.org/10.1039/c6cs00173d.
[13] Z. Song, H. Zhou, Towards sustainable and versatile energy storage devices: an overview of organic electrode materials, *Energ. Environ. Sci.* 6 (2013) 2280–2301, https://doi.org/10.1039/c3ee40709h.
[14] C. Luo, G. Xu, X. Ji, S. Hou, L. Chen, F. Wang, J. Jiang, Z. Chen, Y. Rem, K. Amine, C. Wang, Reversible redox chemistry of azo compounds for sodium-ion batteries, *Angew. Chem.-Int. Ed.* 57 (2018) 2879–2883, https://doi.org/10.1002/anie.201713417.
[15] C. Huang, S. Barlow, S. Marder, Perylene-3,4,9,10-tetracarboxylic acid diimides: synthesis, physical properties, and use in organic electronics, *J. Org. Chem.* 76 (2011) 2386–2407, https://doi.org/10.1021/jo2001963.
[16] C. Chen, X. Zhao, H. Li, F. Gan, J. Zhang, J. Dong, Q. Zhang, Naphthalene-based polyimide derivatives as organic electrode materials for lithium-ion batteries, *Electrochim. Acta* 229 (2017) 387–395, https://doi.org/10.1016/j.electacta.2017.01.172.
[17] K. Oyaizu, A. Hatemata, W. Choi, H. Nishide, Redox-active polyimide/carbon nanocomposite electrodes for reversible charge storage at negative potentials: expanding the functional horizon of polyimides, *J. Mater. Chem.* 20 (2010) 5404–5410, https://doi.org/10.1039/c0jm00042f.
[18] Z. Song, H. Zhan, Y. Zhou, Polyimides: promising energy-storage materials, *Angew. Chem.-Int. Ed.* 49 (2010) 8444–8448, https://doi.org/10.1002/anie.201002439.
[19] H. Wang, S. Yuan, D. Ma, X. Huang, F. Meng, X. Zhang, Tailored aromatic carbonyl derivative polyimides for high-power and long-cycle sodium-organic batteries, *Adv. Energy Mater.* 4 (2014) 1301651, https://doi.org/10.1002/aenm.201301651.
[20] D. Kim, S. Je, S. Sampath, J. Choi, A. Coskun, Effect of N-substitution in naphthalenediimides on the electrochemical performance of organic rechargeable batteries, *RSC Adv.* 2 (2012) 7968–7970, https://doi.org/10.1039/c2ra21239k.
[21] A. Lakraychi, K. Fahsi, L. Aymard, P. Poizot, F. Dolhem, J. Bonnet, Carboxylic and sulfonic N-substituted naphthalene diimide salts as highly stable non-polymeric organic electrodes for lithium batteries, *Electrochem. Commun.* 76 (2017) 47–50, https://doi.org/10.1016/j.elecom.2017.01.019.
[22] S. Renault, J. Geng, F. Dolhem, P. Poizot, Evaluation of polyketones with N-cyclic structure as electrode material for electrochemical energy storage: case of

pyromellitic diimide dilithium salt, *Chem. Commun.* 47 (2011) 2414–2416, https://doi.org/10.1039/c0cc04440g.
[23] Z. Song, T. Xu, M. Gordin, Y. Jiang, I. Bae, Q. Xiao, H. Zhan, J. Liu, D. Wang, Polymer-graphene nanocomposites as ultrafast-charge and -discharge cathodes for rechargeable lithium batteries, *Nano Lett.* 12 (2012) 2205–2211, https://doi.org/10.1021/nl2039666.
[24] M. Veerababu, R. Kothandaraman, Rational functionalization of perylene diimide for stable capacity and long-term cycling performance for Li-ion batteries, *Electrochim. Acta* 232 (2017) 244–253, https://doi.org/10.1016/j.electacta.2017.02.152.
[25] L. Li, H. Gong, D. Chen, M. Lin, Stable bifunctional perylene imide radicals for high-performance organic-lithium redox-flow batteries, *Chem.-a Eur. J.* 24 (2018) 13188–13196, https://doi.org/10.1002/chem.201801443.
[26] L. Li, Y. Hong, D. Chen, W. Xiao, M. Lin, Anion-pi interactions in lithium-organic redox flow batteries, *Chem. Commun.* 55 (2019) 2364–2367, https://doi.org/10.1039/c8cc09834d.
[27] G. Vadehra, R. Maloney, M. Garcia-Garibay, B. Dunn, Naphthalene diimide based materials with adjustable redox potentials: evaluation for organic lithium-ion batteries, *Chem. Mater.* 26 (2014) 7151–7157, https://doi.org/10.1021/cm503800r.
[28] D. Chen, A. Avestro, Z. Chen, J. Sun, S. Wang, X. Min, Z. Erno, M. Algaradah, M. Nassar, K. Amine, Y. Meng, J. Stoddart, A rigid naphthalenediimide triangle for organic rechargeable lithium-ion batteries, *Adv. Mater.* 27 (2015) 2907–2912, https://doi.org/10.1002/adma.201405416.
[29] D. Kim, K. Hermann, A. Prokofjevs, M. Otley, C. Pezzato, M. Owczarek, F. Stoddart, Redox-active macrocycles for organic rechargeable batteries, *J. Am. Chem. Soc.* 139 (2017) 6635–6643, https://doi.org/10.1021/jacs.7b01209.
[30] L. Li, Y. Hong, D. Chen, M. Lin, Molecular engineering of perylene imides for high-performance lithium batteries: diels-alder extension and chiral dimerization, *Chem.-a Eur. J.* 23 (2017) 16612–16620, https://doi.org/10.1002/chem.201703823.
[31] Z. Luo, L. Liu, Q. Zhao, F. Li, J. Chen, An insoluble benzoquinone-based organic cathode for use in rechargeable lithium-ion batteries, *Angew. Chem.-Int. Ed.* 56 (2017) 12561–12565, https://doi.org/10.1002/anie.201706604.
[32] S. Nalluri, Z. Liu, Y. Wu, K. Hermann, A. Samanta, D. Kim, M. Krzyaniak, M. Wasielewski, J. Stoddart, Chiral redox-active isosceles triangles, *J. Am. Chem. Soc.* 138 (2016) 5968–5977, https://doi.org/10.1021/jacs.6b02086.
[33] Z. Cheng, J. Le, J. Wang, W. Sun, L. Zhang, L. Cai, D. Lu, Y. Shen, J. Wu, F. Fu, H. Chen, Self-activation enables cationic and anionic co-storage in organic frameworks, *Adv. Energy Mater.* 12 (2022) 2101930, https://doi.org/10.1002/aenm.202101930.
[34] W. Sun, C. Zhou, Y. Fan, Y. He, H. Zhang, Z. Quan, H. Kong, F. Fu, J. Qin, Y. Shen, H. Chen, Ion Co-storage in porous organic frameworks through on-site coulomb interactions for high energy and power density batteries, *Angew. Chem.-Int. Ed.* 62 (2023) e2023001, https://doi.org/10.1002/anie.202300158.
[35] J. Russell, V. Posey, J. Gray, R. May, D. Reed, H. Zhang, L. Marbella, M. Steigerwald, Y. Yang, X. Roy, C. Nuckolls, S. Peurifoy, High-performance organic pseudocapacitors via molecular contortion, *Nat. Mater.* 20 (2021) 1136–1141, https://doi.org/10.1038/s41563-021-00954-z.
[36] L. Oleksii, T.H. Jochem, R. Petra, F. Ben, B. Wesley, Oxidative electrochemical aryl C-C coupling of spiropyrans, *Chem. Commun.* 49 (2013) 6737–6739, https://doi.org/10.1039/c3cc42396d.
[37] O. Ivashenko, J. van Herpt, P. Rudolf, B. Feringa, W. Browne, Oxidative electrochemical aryl C-C coupling of spiropyrans, *Chem. Commun* 49 (2013) 6737–6739, https://doi.org/10.1039/c3cc42396d.
[38] T. Mizoguchi, R. Adams, Anodic oxidation studies of N,N-dimethylaniline. I. Voltammetric and spectroscopic investigations at platinum electrodes, J. Am. Chem. Soc. 84 (1962) 2058–2061, https://doi.org/10.1021/ja00870a009.
[39] Z. Galus, R. White, F. Rowland, R. Adams, Anodic oxidation studies of N,N-dimethylaniline. III. Tritium tracer studies of electrolysis products, J. Am. Chem. Soc. 84 (1962) 2065–2068, https://doi.org/10.1021/ja00870a011.
[40] J. Tanaka, S. Nagakura, M. Kobayashi, Ultraviolet and infrared absorption spectra of substituted acetophenones and benzoic acids, *J. Phys. Chem. C* 24 (1956) 311–315, https://doi.org/10.1063/1.1742469.
[41] L. Jie, W. Yao, Y. Meng, Y. Yang, Effects of vinyl ethylene carbonate additive on elevated-temperature performance of cathode material in lithium ion batteries, *J. Phys. Chem. C* 112 (2008) 12550–12556, https://doi.org/10.1021/jp800336n.
[42] J. Wang, J. Polleux, J. Lim, B. Dunn, Pseudocapacitive contributions to electrochemical energy storage in TiO_2 (anatase) nanoparticles, *J. Phys. Chem. C* 111 (2007) 14925–14931, https://doi.org/10.1021/jp074464w.
[43] Y. Wang, P. Poldorn, Y. Wongnongwa, S. Jungsuttiwong, C. Chen, L. Yu, Z. Wang, L. Shi, Y. Zhao, S. Yuan, Cobalt(II)-hexaazatriphenylene hexacarbonitrile coordination compounds based cathode materials with high capacity and long cycle stability, *Adv. Funct. Mater.* 32 (2022), https://doi.org/10.1002/adfm.202111043.
[44] H. Zhang, Y. Zhang, C. Gu, Y. Ma, Electropolymerized conjugated microporous poly(zinc-porphyrin) films as potential electrode materials in supercapacitors, *Adv. Energy Mater.* 5 (2015), https://doi.org/10.1002/aenm.201402175.
[45] F. Xu, H. Wang, M. Wu, J. Nan, T. Li, S. Cao, Electrochemical properties of poly (anthraquinonyl imide)s as high-capacity organic cathode materials for Li-ion batteries, *Mater. Chem. Phys.* 1 (2018) 120–125, https://doi.org/10.1016/j.matchemphys.2018.04.079.
[46] H. Wu, Q. Meng, Q. Yang, M. Zhang, K. Lu, Z. Wei, Large-area polyimide/SWCNT nanocable cathode for flexiblelithium-ion batteries, *Adv. Mater.* 27 (2015) 6504–6510, https://doi.org/10.1002/adma.201502241.